Miscible Displacements with a Chemical Reaction in a Capillary Tube

Yuichiro Nagatsu, Yuji Hosokawa, Yoshihito Kato, and Yutaka Tada
Dept. of Materials Science and Engineering, Graduate School of Engineering, Nagoya Institute of Technology, Gokiso-cho, Showa-ku, Nagoya, Aichi 466-8555, Japan

Toshihisa Ueda
School of Science for Open and Environmental Systems, Keio University, 3-14-1 Hiyoshi, Kouhoku-ku, Yokohama, Kanagawa 223-8522, Japan

DOI 10.1002/aic.11407
Published online January 11, 2008 in Wiley InterScience (www.interscience.wiley.com).

Miscible displacement of a more-viscous liquid by a less-viscous one with a chemical reaction in a capillary tube was investigated experimentally and theoretically. In such a flow field, the less-viscous liquid continuously leaks from the tip of the finger-shaped boundary between the two liquids to form another thin finger depending on flow condition. This is called a "spike." Experimental results show that in the spike product is clearly or scarcely observed when the initial reactant concentration in the less-viscous liquid is sufficiently larger or smaller than the stoichiometry, respectively. On the basis of theoretical results, a model is proposed in which the difference in the reaction plane's location in either the less-viscous liquid or in the boundary (determined by the variation in the initial reactant concentrations) results in a significant difference between the locations of the boundary and the reaction plane, this difference being affected by the spike configuration of the boundary. © 2008 American Institute of Chemical Engineers *AIChE J,* 54: 601–613, 2008

Keywords: miscible displacement, spike formation, reacting flow, convection-diffusion-reaction analysis, viscous fingering

Introduction

Displacement in porous media

The displacement of one viscous fluid by another in a porous medium is an important process with a variety of applications, for example, in enhanced oil recovery, fixed bed regeneration, hydrology, and filtration. Basic stability theory[1,2] informs us that if the displacing fluid is less viscous than the displaced fluid, the resulting unfavorable mobility profile will lead to the well-known phenomenon of fingering instability, which causes the displacing fluid to channel through the displaced zone, thereby reducing the efficiency of the displacement process. If the fluids are of different densities, gravity can exert an additional stabilizing or destabilizing influence. Depending on whether the two fluids are immiscible or miscible, one can distinguish two apparently different problems. In the immiscible case, in which the interfacial tension acts at the interface between the two fluids, the capillary number, which is the ratio of viscous to interfacial tension forces, represents a dynamically important parameter. In the miscible case, the dynamically important parameter is the Péclet number, which is defined as the ratio of the convective to diffusive transport rate of mass. As the pore-level details of such flows in a real porous medium are too complicated to measure experimentally and to simulate

Correspondence concerning this article should be addressed to Y. Nagatsu at nagatsu@nitech.ac.jp.

numerically, the flow in simple geometries, such as those within capillary tubes or between closely spaced parallel plates (as in a Hele-Shaw cell), has been used to model certain aspects of these flows. The former is usually considered the simplest model of displacement in a single pore of such a medium, while the latter could be considered a limiting model for two-dimensional motion in an extended porous medium.

Displacement in capillary tubes

Earlier studies regarding displacement in capillary tubes have been devoted to the immiscible case. A main interest of these studies is the fraction of the displaced fluid left behind on the tube walls, m. Taylor[3] studied the displacement of a viscous fluid by another immiscible fluid (air) in a horizontal capillary tube and found that the relationship between m and the capillary number, $Ca = V_t\mu_2/\sigma$ (where V_t is the velocity of the tip, μ_2 is the viscosity of the displaced fluid, and σ is the surface tension between the displaced fluid and the displacing air) shows a single curve for a number of fluids, with this curve increasing from the origin as $Ca^{0.5}$ for small Ca, and reaching a value of 0.56 for moderately large Ca. In a later experiment, Cox[4] extended the range of Ca and found an apparent asymptotic of 0.60 at large Ca. The corresponding numerical simulations reported by Reinelt and Saffman[5] agree closely with the results of these experiments.

Experiments by Petitjeans and Maxworthy[6] extended Taylor[3] by using two miscible fluids (glycerin and glycerin/water mixtures) in capillary tubes. Corresponding numerical simulations were performed by Chen and Meiburg[7] as well. Petitjeans and Maxworthy[6] found that for a large Péclet number, Pe, the fraction m was found to depend only on the Atwood number, At. Here, the Péclet number is defined as $Pe = V_m d/D$, where V_m is the mean velocity of the Poiseuille flow ahead of the fingertip, d is the tube diameter, and D is a suitably averaged diffusion coefficient. As well, the Atwood number, At, is defined as $At = (\mu_2 - \mu_1)/(\mu_2 + \mu_1)$ and thus is a measure of the contrast of viscosity between the two fluids, where μ_1 is the viscosity of the displacing fluid. When At tended to unity, the fraction m increased to a value of 0.61, which is virtually identical to the value of 0.60 obtained by Cox[4] for immiscible displacements. For a small Pe, Petitjeans and Maxworthy[6] found that the fraction m depended strongly on At and a gravitational parameter, $F = gd^2(\rho_1 - \rho_2)/\mu_2 V_m$, which represents the relative importance of the gravitational and viscous force, where g is the gravitational acceleration, and ρ_1 and ρ_2 are the densities of the less- and more-viscous liquids, respectively. The parameter F is negative if gravitational effects stabilize the finger displacement and positive if they destabilize it. It has been demonstrated that the less-viscous fluid continuously leaks from the fingertip to form another thinner finger depending on flow conditions when $m < 0.5$. This is called a "spike." The spike never appears in the immiscible cases, in which the interface is parabolic regardless of flow condition. The miscible displacement of the less-viscous liquid by the more-viscous liquid has been recently studied by Balasubramaniam et al.,[8] who observed that the boundary between the two liquids exhibits an asymmetric, sinuous shape as well as spike, depending on the flow conditions.

Displacement in Hele-Shaw cells

In studies of displacement in Hele-Shaw cells, three main types of geometries have been used, these being rectilinear, radial, and five-spot geometries.[9] Studies of the displacement in Hele-Shaw cells can be divided into two categories. One category regards the dynamics of the interface or boundary in the L (length) $\times$ W (width) plane for rectilinear displacements or in the R (radius) $\times$ θ plane for radial or five-spot displacements. The other category regards the shape of the interface or boundary in the cell's gap, that is, in the $L \times b$ (thickness of the cell's gap) plane or the $R \times b$ plane. In the former case, a nonlinear propagation of viscous fingering has been exhaustively studied and is well understood especially in Newtonian fluids. The nonlinear propagation of viscous fingering is governed by different mechanisms of shielding, spreading, and splitting. Shielding is a phenomenon in which a finger slightly ahead of its neighboring fingers quickly outruns them and shields them from further growth. Spreading and splitting are phenomena, in which a finger that spreads until it reaches a certain width, becomes unstable and splits.[9] A few studies regarding the latter type for immiscible displacement have been reported. It has been found that when capillary force across the gap is large enough to ensure the complete separation of the immiscible fluids, the meniscus then spans the gap, having a semispherical shape at sufficiently small capillary numbers.[10] At a sufficiently high flow rate, however, where capillarity is small, the interface separating the two immiscible fluids does not span the gap and may develop within the gap itself.[11] This latter type of study regarding miscible displacement has been recently reported. Several researchers have shown both theoretically and numerically that miscible displacement can be described as an advancing front with a well-defined interface, propagating symmetrically in the middle of the gap, provided that the flow velocity is large enough for diffusive effects to be negligible.[12–14] Lajeunesse et al.[15] experimentally showed three types of interface shape depending on the viscosity ratio and flow rate in vertical displacements, referring to them as the absence of shock, the presence of an internal shock, and the presence of a frontal shock. Here, "shock" means an abrupt decrease in the thickness of the less-viscous liquid layer in the direction of the cell's gap. This type of internal shock corresponds to the spike observed in the miscible displacement in the capillary tube. The internal shock-type structure has been demonstrated by a recent numerical simulation.[16]

Viscous fingering with chemical reactions

It has been reported that the viscous fingering phenomenon accompanied by chemical reactions can be observed in processes such as petroleum recovery,[17] chromatographic and adsorptive separation,[18] polymerization,[19] and the flow of gastric mucus[20] and has been confirmed as playing an important role in these processes. Therefore, the coupling between hydrodynamics and chemistry in viscous fingering involving chemical reactions has been a subject of study. Fernandez and Homsy[21] performed experiments on immiscible viscous fingering involving a chemical reaction acting to reduce interfacial tension in a radial Hele-Shaw cell, finding that the reaction makes the fingers wider. They characterized the effects of the reaction on the reactive fingering pattern in

terms of the Damköhler number, *Da*, which is defined as the ratio between the characteristic time of fluid motion and that of a chemical reaction. DeWit and Homsy[22,23] performed a numerical simulation on reactive miscible viscous fingering in two-dimensional rectilinear porous media by assuming that the fluid's viscosity is a function of a chemical species concentration and by using a specific chemical kinetics. They found a new mechanism of viscous fingering, which they refer to as the "droplet" mechanism, which involves the formation of isolated regions of either less- or more-viscous fluids in connected domains of the other. Nagatsu et al.[24] performed experiments on miscible viscous fingering involving instantaneous chemical reactions that increase or decrease the viscosity of the more-viscous fluids in a radial Hele-Shaw cell. They found that the shielding effect is suppressed and the fingers are widened when the viscosity of the more-viscous fluid is increased by the reaction. In contrast, the shielding effect is enhanced and the fingers are narrowed when the viscosity of the more-viscous fluid is decreased by the reaction. These studies[21–24] investigated a chemical reaction's effect on the viscous fingering pattern in the $L \times W$ plane or the $R \times \theta$ plane.

The authors' previous studies on miscible viscous fingering (or miscible displacement) with a chemical reaction in a Hele-Shaw cell and the motivation of the present study

Nagatsu and Ueda[25] performed experiments on reactive miscible viscous fingering (or reactive miscible displacement) in a radial Hele-Shaw cell in a case in which the finger-growth velocity (or the displacement velocity) is low. In their experiments, a 99 wt % glycerin solution that included potassium thiocyanate (KSCN) and an iron nitrate [$Fe(NO_3)_3$] solution were used as the more- and less-viscous liquids, respectively. The instantaneous chemical reaction expressed in Eq. 1 takes place, resulting in a blood red-colored product.

$$Fe^{3+} + 2SCN^- \rightarrow [Fe(SCN)_2]^+(\text{blood red}). \tag{1}$$

This reaction has no influence on the hydrodynamics of the fingering. It was shown that the product distribution in the viscous fingering pattern in the $R \times \theta$ plane is highly dependent on the ratio between the reactant concentrations initially included in the more- and less-viscous liquids normalized by a stoichiometric ratio of the chemical reaction, ϕ_v, which is expressed as Eq. 2,

$$\varphi_v = \frac{ac_{l0}}{c_{m0}}. \tag{2}$$

In this equation, c_{l0} and c_{m0} are the molar reactant concentrations initially included in the less- and more-viscous liquids, respectively, and a is the molar stoichiometric ratio of the chemical reaction, which is $a = 2$ in this study, as shown in Eq. 1. For $\varphi_v \ll 1$, the product is present in large quantities in a relatively broad area within the interior of the fingers, while for $\varphi_v \gg 1$, it is concentrated around the tips of the fingers. For $\varphi_v = 1$, the product is equally distributed among the interiors and tips of the fingers. Nagatsu and Ueda[25] also theoretically analyzed the transport of the reactants and the product in two miscible liquids employed in their experiment, that is, a 99 wt % glycerin solution (the more-viscous liquid) and water (the less-viscous liquid), by using a one-dimensional steady state diffusion-reaction model with the assumption of a distinct interface between the two miscible liquids. The analytical results revealed that for $\varphi_v \ll 1$, the reaction plane is located in the less-viscous liquid far from the interface between the two liquids and the product widely diffuses in the diffusive zone of the less-viscous liquid. On the other hand, for $\varphi_v \gg 1$, the reaction plane is located in the more-viscous liquid close to the interface and the product concentrates close to the interface in the more-viscous liquid. Therefore, it was concluded that the experimentally observed product distribution is caused by the difference in the location of the reaction planes and the difference in the product distributions in the diffusive zone due to φ_v.

Next, Nagatsu and Ueda[26] experimentally showed that the dependence on φ_v of the product distribution in the fingering pattern in the $R \times \theta$ plane decreases with an increase in the finger-growth velocity. Under the condition of high finger-growth velocity, the product is distributed from the interior to the tip of the fingers regardless of φ_v. A possible reason for this was suggested as follows. For $\varphi_v \ll 1$, the location of the reaction plane is shifted in the less-viscous liquid toward the interface and the product is significantly distributed around the interface due to convective effects, as compared to the case of the low finger-growth velocity. In contrast, for $\varphi_v \gg 1$, the location of the reaction plane and the product distribution do not significantly vary even as the finger-growth velocity increases. As a result, the reaction plane is located close to the interface and the product is significantly distributed around the interface without regard to φ_v when the finger-growth velocity is high. Subsequently, Nagatsu and Ueda[27] performed a theoretical analysis that added convective effects to the previous diffusion-reaction analysis to theoretically verify the mechanism suggested above. In the convection-diffusion-reaction analysis model, a two-dimensional stagnated flow field is assumed in the less-viscous liquid whereas no flow is assumed in the more-viscous liquid because it is proposed that when the less-viscous liquid displaces the more-viscous liquid, the flow of the less-viscous liquid around the interface is stagnated owing to the large difference in the viscosities of the two liquids.[28] Under the assumption of the two-dimensional stagnated flow field, the conservation equations of the reactants and the product become one-dimensional. The obtained analytical results supported the proposed mechanism described earlier.

The nonreactive experiment reported by Nagatsu and Ueda[25] showed that the color of the dyed less-viscous liquid in the viscous fingering pattern in the $R \times \theta$ plane becomes abruptly light at the fingertips. The authors suggested that this is caused by the thickness of the less-viscous liquid layer in the cell's gap direction (in the $R \times b$ plane) becoming abruptly thin at the fingertips, which is analogous to the spike observed in miscible displacement in a capillary tube. Here, the proposed structure of the fingertips in the Hele-Shaw cell is referred as to a "sheet structure." The nonreactive experiment reported by Nagatsu and Ueda[26] showed that the sheet structure disappears when the finger-growth velocity is high. In previous studies,[25,26] the relationship between the dependence of the product distribution on φ_v and the

sheet structure has not been explicitly discussed. This is the motivation of the present study. In other words, the present study focuses on whether the significant difference in the product distribution due to the initial reaction concentrations is caused by the formation of the sheet structure in the miscible displacement in the Hele-Shaw cell or the formation of the spike in the miscible displacement in the capillary tube. Investigation of the reacting flow field in the $L \times b$ plane or the $R \times b$ plane is difficult when using a Hele-Shaw cell. In the present study, in order to elucidate the relationship between the spike structure and the product distribution's dependence on the initial reactant concentration, experiments have been performed regarding miscible displacement involving a spike with a chemical reaction in a capillary tube, using the same liquids and chemical reaction as those employed in Nagatsu and Ueda.[25,26] From recent studies,[6,15,29] we know that a spike can form under a certain condition when a lighter less-viscous liquid downwardly displaces a heavier more-viscous liquid in a vertical capillary tube. We first performed preliminary nonreactive experiments by using the experimental set-up mentioned above in an attempt to determine the fluid dynamical condition under which the spike is formed. After that, reactive experiments were performed under a condition involving the spike by varying the initial reactant concentrations. For the sake of comparison with the case involving the spike, reactive experiments were also performed under a condition in which the spike is not formed.

As mentioned earlier, we performed a theoretical analysis of the transport of the reactants and product in two miscible liquids employed in a reactive miscible viscous fingering experiment, that is, a 99 wt % glycerin solution (the more-viscous liquid) and water (the less-viscous liquid), assuming a distinct interface between the two miscible liquids.[25,27] Here, we recall that in the previous analysis, a distinct interface between the two miscible liquids was assumed. This means that although the two miscible-liquid system contains three regions (namely a less-viscous liquid region, a more-viscous liquid region, and a boundary region between the more- and less-viscous liquids), the presence of the boundary region was ignored (Refer to Figure 6, which will be discussed in detail later). This also means that the miscibility between the two liquids was not taken into account; in other words, diffusion between less- and more-viscous liquids was ignored. As will be discussed in detail later in this article, the diffusion coefficient between the solvents of the less-viscous liquid (water) and of the more-viscous liquid (99 wt % glycerin solution) is larger than that of the reactants and the product with sufficiently small concentrations compared to the solvent concentration in the more-viscous liquid (99 wt % glycerin solution). This is not consistent in the previous analysis, in which the diffusion between the more- and less-viscous solvents was ignored although the diffusion of the reactants and the product in the more-viscous solvent was taken into account. In the present article, we develop an improved version of the theoretical analysis employed in Nagatsu and Ueda[25,27] by taking into account the miscibility of the more- and less-viscous solvents. Finally, the reacting flow field employed in the present study is discussed based on the results obtained in the present theoretical analysis.

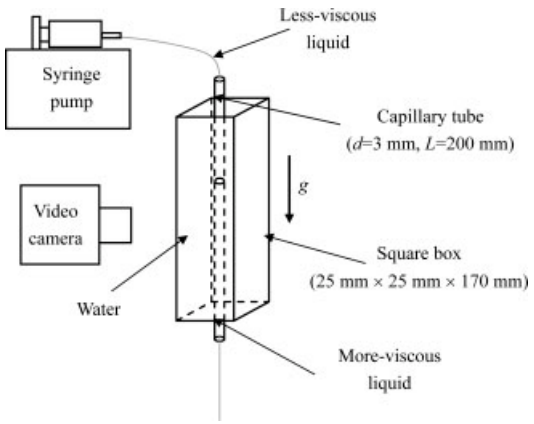

Figure 1. Experimental apparatus.

The lighter less-viscous liquid downwardly displaces the heavier more-viscous liquid.

Experimental

Experimental apparatus and method

Figure 1 shows the experimental apparatus. A capillary tube with an inner diameter $d = 3$ mm and a length $L = 200$ mm was positioned vertically. First, the capillary tube was filled to the desired level with the more-viscous liquid from the bottom of the tube. After the less-viscous liquid was gently added from the top of the tube manually, the less-viscous liquid was then injected at a constant volumetric flow rate by a syringe pump. To reduce optical distortions, the cylindrical tube was surrounded by a square box and the intervening space was filled with water, thus attempting to match the refractive index. The displacement patterns observed were recorded by a digital video camera.

Liquids and chemical reaction

Experiments were performed for the reactive and nonreactive cases. The liquids and chemical reaction used in the reactive cases were the same as those used in the study by Nagatsu and Ueda.[25,26] Hence, a 99 wt % glycerin solution that included KSCN (colorless) and an iron nitrate [$Fe(NO_3)_3$] solution (light yellow) were used as the more- and less-viscous liquids, respectively. Therefore, the chemical reaction expressed by Eq. 1 takes place. In the present study, the dimensionless parameter, φ, defined in Eq. 2, is introduced here as well as in the study by Nagatsu and Ueda[25] in which subscript v is omitted because it indicated viscous fingering. The experiments were performed under a condition in which φ is set as 0.04, 0.2, 1, 5, and 25. The initial reactant concentration in the less-viscous liquid, c_{l0}, and that in the more-viscous liquid, c_{m0}, for each experiment are shown in Table 1. Here, c_{l0} and c_{m0} are determined as the product concentration at the reaction plane are identical for each φ condition (See Appendix). For the nonreactive cases, a 99 wt % glycerin solution and a 1 wt % methylene blue solution were used as the more- and less-viscous liquids, respectively.

On parameters

As mentioned in "Introduction", it is known that for miscible displacements in capillary tubes flow characteristics are

Table 1. Combinations of c_{l0} and c_{m0} for Various φ Conditions

Condition	c_{l0} (mol/L)	c_{m0} (mol/L)
$\varphi = 0.04$	0.00473	0.236
$\varphi = 0.2$	0.00545	0.0545
$\varphi = 1$	0.00909	0.0182
$\varphi = 5$	0.0273	0.0109
$\varphi = 25$	0.118	0.00945

governed by three nondimensional parameters: the Atwood number, *At*, the Péclet number, *Pe*, and a gravitational parameter, *F*, which are defined by Eqs. 3–5, respectively,

$$At = \frac{\mu_2 - \mu_1}{\mu_2 + \mu_1}, \tag{3}$$

$$Pe = \frac{Ud}{D}, \tag{4}$$

$$F = \frac{gd^2(\rho_1 - \rho_2)}{\mu_2 U}. \tag{5}$$

Here, μ_1 and μ_2 are the viscosities of the less- and more-viscous liquids, having values of 0.001 and 1 Pa s, respectively. In Eq. 4, *D* represents an average diffusivity between glycerin and water and has a value of 1.6×10^{-10} m^2/s, as measured by Petitjeans and Maxworthy.[6] In Eq. 5, ρ_1 and ρ_2 are the densities of the less- and more-viscous liquids, respectively. The characteristic velocity, *U*, is defined in the present study as

$$U = \frac{q}{\left(d/2\right)^2 \pi}, \tag{6}$$

where *q* is the volumetric injection rate of the less-viscous liquid.

Experimental Results

On the case in the presence of the spike

We first present the experimental results by setting $q = 7.76 \times 10^{-10}$ m^3/s as the condition in which the spike is formed. The values of the three nondimensional parameters and those of ρ_1 and ρ_2 for each φ condition under this experimental condition of *q* are summarized in Table 2. As shown in Table 2, *At* and *Pe* are independent of φ and have constant values. Although *F* varies from -225 to -184 depending on the condition of φ, this variation is considered to be small; therefore, the flow characteristics for each condition of φ are considered to be unchanged. Figure 2 shows the miscible displacement pattern in the nonreactive case, where the injection time of the less-viscous liquid, *t*, is 480 s. We confirmed that under the present experimental conditions, the boundary between the two liquids forms a spike. Figure 3 shows experimental results with the chemical reaction for various φ conditions at $t = 480$ s. The blood-red color indicates the presence of the product and the color depth corresponds to the product's concentration. The product's distribution significantly varies by φ. When φ is smaller than unity ($\varphi = 0.04$ and 0.2), the product is scarcely observed in the region where the spike is observed in the nonreactive experiment. As mentioned above, the flow characteristics in these reactive conditions are unchanged compared to the nonreactive case. This shows that although the spike is formed, the product is not distributed in the spike. It should be noted that in these cases, the spike is never visible as the original color of the less-viscous liquid because the less-viscous liquid is almost colorless. [In the reactive experiments, the less-viscous liquid is the $(Fe(NO_3)_3)$ solution whose color is light yellow. As its concentration is smaller, the depth of the color is lighter. For small φ, the concentration of the $Fe(NO_3)_3$ is small, thus the $Fe(NO_3)_3$ solution becomes almost colorless.] When φ is larger than unity ($\varphi = 5$ and 25), the product is obviously observed in the spike. When φ is unity, the product distribution takes a middle state between the conditions where φ is smaller and larger than unity. We have found that the depth of the blood-red color around the base of the finger in each experiment is almost identical. This is because c_{m0} and c_{l0} were set such that the product's concentration at the reaction plane is identical for each φ condition.

On the cases in the absence of the spike

We have found that the spike does not form when *q* is decreased or increased from the value mentioned above. We have conducted reactive experiments varying *q* under the conditions of $\varphi = 0.04$ and 25 in order to examine whether the spike is responsible for the significant dependence of the product distribution on φ. Figure 4 shows the miscible displacement without and with the reaction for the condition of $q = 1.55 \times 10^{-10}$ m^3/s at $t = 480$ s, which is a smaller *q* case compared to the case in the presence of the spike. In this case, $Pe = 657$ and *F* is -1010 for the nonreactive case, -1130 for the case of $\varphi = 0.04$, and -926 for the case of $\varphi = 25$. In the nonreactive case, the spike is not formed and the shape of the displacement tip is almost parabolic. In the reactive cases, the difference in the product distribution as induced by variations in φ is hardly observed. Figure 5 shows the miscible displacement without and with the reaction for the condition of $q = 1.05 \times 10^{-8}$ m^3/s at $t = 30$ s, which is a larger *q* case compared to be the case in the presence of the spike. In this case, $Pe = 4.47 \times 10^4$ and *F* is -14.8 for the nonreactive case, -16.6 for the case of $\varphi = 0.04$, and -13.6 for the case of $\varphi = 25$. In the nonreactive case, the spike is not formed and the shape of the displacement tip is also almost parabolic. In the reactive cases, no difference in the product distribution as induced by φ is observed.

Table 2. Values of *At*, *Pe*, and *F* Along With ρ_1 and ρ_2 for the Various Experimental Conditions Under the Condition of $q = 7.76 \times 10^{-10}$ m^3/s

Condition	ρ_1 (kg/m^3)	ρ_2 (kg/m^3)	*At*	*Pe*	*F*
Nonreactive	1.01×10^3	1.26×10^3	0.998	3300	-200
$\varphi = 0.04$	1.00×10^3	1.28×10^3	0.998	3300	-225
$\varphi = 0.2$	1.00×10^3	1.26×10^3	0.998	3300	-208
$\varphi = 1$	1.00×10^3	1.26×10^3	0.998	3300	-208
$\varphi = 5$	1.01×10^3	1.26×10^3	0.998	3300	-200
$\varphi = 25$	1.03×10^3	1.26×10^3	0.998	3300	-184

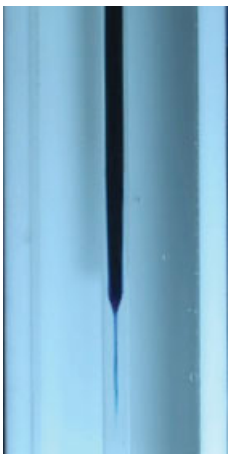

Figure 2. Miscible displacement pattern in the nonreactive case at t = 480 s under the conditions of At = 0.998, Pe = 3300, and F = −200.

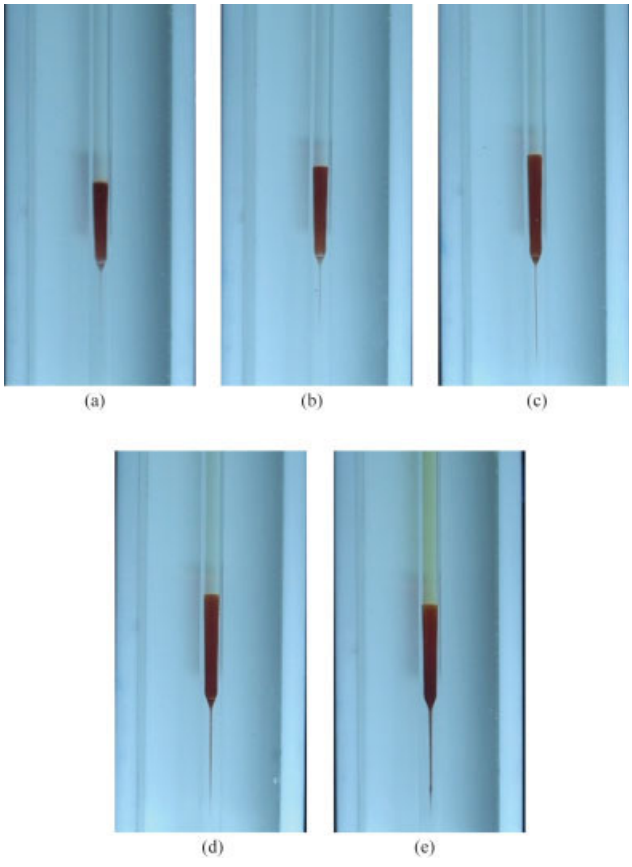

Figure 3. Miscible displacement patterns in the reactive case at t = 480 s under the conditions of At = 0.998, Pe = 3300, and F = −225 to −184 for various φ, (a) φ = 0.04, (b) φ = 0.2, (c) φ = 1, (d) φ = 5, and (e) φ = 25.

The blood-red color indicates the product's presence and the color depth corresponds to the product's concentration.

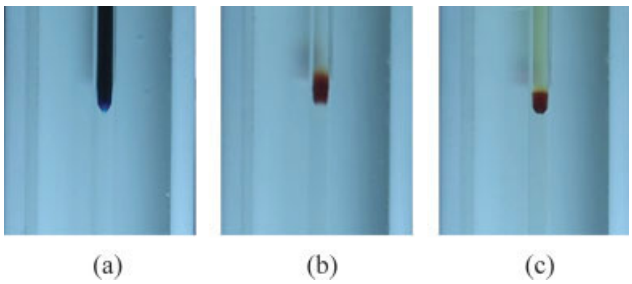

Figure 4. Miscible displacement for (a) the nonreactive case, (b) φ = 0.04, and (c) φ = 25 at t = 480 s under the conditions of At = 0.998, Pe = 657, and F = −1130 to −926.

Theoretical Analysis of the Transport of the Reactants and the Product

As mentioned in "Introduction", although the theoretical analyses performed by Nagatsu and Ueda[25,27] assumed a distinct interface between the two miscible liquids, this assumption involved a discrepancy. In the present article, an extended version of the theoretical analyses performed by Nagatsu and Ueda[25,27] has been developed by taking miscibility into account.

Figure 6 shows a schematic of the one-dimensional profile of the mass fractions of the reactants initially included in the miscible less-viscous liquid (water) and the more-viscous liquid (99 wt % glycerin solution), Y_l and Y_m, respectively. The two miscible-liquid system contains three regions: namely, a less-viscous liquid region ($\tilde{x} \leq \tilde{x}_{b-}$), a more-viscous liquid region ($\tilde{x}_{b+} \leq \tilde{x}$), and a boundary region between the more- and less-viscous liquids ($\tilde{x}_{b-} \leq \tilde{x} \leq \tilde{x}_{b+}$), in which $\tilde{x}_{b-}$ and $\tilde{x}_{b+}$ represent the edges at the less- and more-viscous liquid sides of the boundary region, respectively. Since the more- and less-viscous solvents are 99 wt % glycerin solutions and water, the weight concentration of glycerin, denoted as w, varies monotonically from 0 to 99 wt % in the boundary

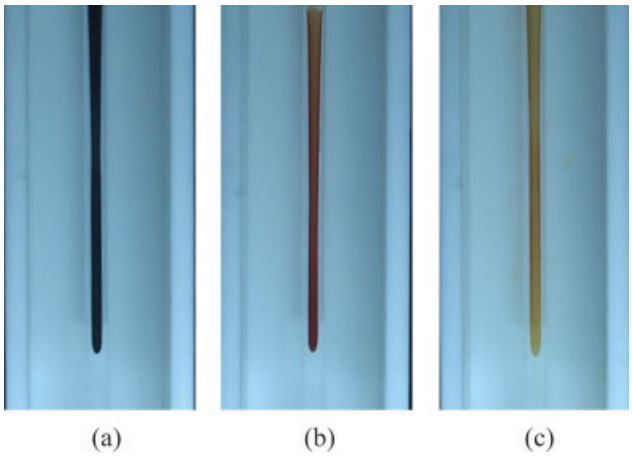

Figure 5. Miscible displacement for (a) the nonreactive case, (b) φ = 0.04, and (c) φ = 25 at t = 30 s under the conditions of At = 0.998, Pe = 4.47 × 10^4, and F = −16.6 to −13.6.

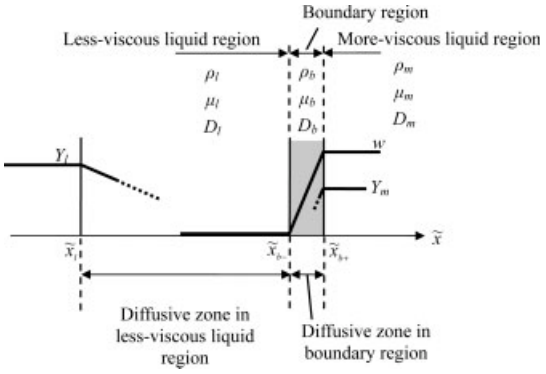

Figure 6. Schematic of one-dimensional profiles of the mass fractions of the reactants initially included in the miscible less-viscous liquid (water) and more-viscous liquid (99 wt % glycerin solution).

Y_l and Y_m are the mass fractions of the reactants initially included in the miscible less-viscous liquid and the more-viscous liquid, respectively. w is the weight concentration of glycerin. ρ_l and μ_l are the density and viscosity of the less-viscous liquid, respectively, and D_l is the diffusion coefficient of the reactants and the product in the less-viscous liquid region. ρ_m, μ_m, and D_m are those for the more-viscous liquid region and ρ_b, μ_b, and D_b are those for the boundary region. $\tilde{x}_l$ indicates the edge of the diffusion zone of the reactants and the product in the less-viscous liquid. $\tilde{x}_{b-}$ and $\tilde{x}_{b+}$ represent the edges at less- and more-viscous liquid sides of the boundary region, respectively.

region. Here, for the sake of simplicity, the profile of w is shown linearly. The density and viscosity of the less-viscous liquid are designated as ρ_l and μ_l, respectively, and the diffusion coefficient of the reactants and the product in the less-viscous liquid region with a sufficiently low concentration (this condition is satisfied in the present experiments) is designated as D_l. Those for the more-viscous liquid region are designated ρ_m, μ_m, and D_m, and those in the boundary region are designated ρ_b, μ_b, and D_b, respectively. Here, μ_l and μ_m are set to 0.001 and 1 Pa s. The diffusion coefficient of the chemical species in a solvent with a sufficiently low concentration is inversely proportional to the solvent viscosity under a constant temperature.[30] In the case in which the solvent is water, the diffusion coefficient has an order of magnitude of 10^{-9} m^2/s.[31] As a result, D_l and D_m are estimated to be 10^{-9} and 10^{-12} m^2/s, respectively. The average diffusion coefficient of the miscible 99 wt % glycerin solution (the more-viscous liquid) and water (the less-viscous liquid), D_{gw}, can be estimated to be $D_{gw} \approx 10^{-10}$ m^2/s based on the measured value reported by Petitjeans and Maxworthy.[6] This indicates that the width of the reactants' and product's diffusion zone (diffusion width) in the less-viscous liquid region is much larger than that in the boundary region of the less- and more-viscous liquids. In contrast, the diffusion width of the reactants and the product in the more-viscous liquid region is much smaller than that in the boundary region, indicating that the reactant initially included in the more-viscous liquid diffuses in the boundary region at the rate at which the more- and less-viscous liquids diffuse. These are schematically shown in Figure 6; as the edge of the diffusion zone of the reactants and the product in the less-viscous liquid is represented by $\tilde{x}_l$, the relation $\tilde{x}_l < \tilde{x}_{b-}$ is satisfied, and Y_m is varied in $\tilde{x} < \tilde{x}_{b+}$. In other words, Y_l and Y_m vary in the region of $\tilde{x}_l \le \tilde{x} \le \tilde{x}_{b+}$. Consequently, the convection diffusion-reaction in $\tilde{x}_l \le \tilde{x} \le \tilde{x}_{b+}$ is discussed below. In the present study, ρ_l is assumed to be constant and to have a value of $\rho_l = 1.0 \times 10^3$ kg/m^3. A constant value of $\rho_b = 1.0 \times 10^3$ kg/m^3 is assumed, although ρ_b is considered to vary about 30% in the range $\rho_b = 1.0$–1.3×10^3 kg/m^3. Thus, $\rho_l = \rho_b = 1.0 \times 10^3$ kg/m^3 $= \rho$ is satisfied. For diffusion coefficients, D_l is assumed to be constant and to have a value of $D_l = 1 \times 10^{-9}$ m^2/s. As mentioned above, it is appropriate that D_b is considered equal to D_{gw}; thus, D_b is assumed to be constant and to have a value of $D_b = 1 \times 10^{-10}$ m^2/s.

In the present analysis as well as that of Nagatsu and Ueda,[27] the flow in the less-viscous liquid region $(\tilde{x}_l \le \tilde{x} \le \tilde{x}_{b-})$ is modeled as a two-dimensional, steady, stagnated flow in which velocities in the $\tilde{x}$- and $\tilde{y}$-directions, represented as V_x and V_y respectively, are expressed as $V_x = -K(\tilde{x} - \tilde{x}_{b-})$ and $V_y = K\tilde{y}$, where K is constant.[32] In addition, no flow is assumed in the boundary region $(\tilde{x}_{b-} \le \tilde{x} \le \tilde{x}_{b+})$. Under the two-dimensional stagnated flow field mentioned above, scalar gradients in the $\tilde{y}$-direction are absent[27,33]; this permits the conservation equations of the reactants and the product to become one-dimensional. Furthermore, as in Nagatsu and Ueda[25,27] as well, an instantaneous chemical reaction and Fick's law of diffusion are assumed. Figures 7a,b show schematics of a mass fraction model of the two reactants and the product in the case in which the location of a reaction plane, $\tilde{x}_r$, is in the less-viscous liquid region $(\tilde{x}_l \le \tilde{x}_r \le \tilde{x}_{b-})$ and in the boundary region $(\tilde{x}_{b-} \le \tilde{x}_r \le \tilde{x}_{b+})$, respectively. In these figures, the mass fraction profiles are represented by straight lines, indicating a case involving no convective effect. At $\tilde{x} = \tilde{x}_r$, the reaction rate is infinite, and no reactants are assumed to exist there. The present analysis assumes the continuities of mass fractions and the mass fluxes of the reactants and the product at $\tilde{x} = \tilde{x}_{b-}$. Under the assumption of the two-dimensional, steady, stagnated flow in the less-viscous liquid, the profile of the velocity toward the boundary, u, is linear in relation to $\tilde{x}$ as shown in Figure 7c, where u_0 is u at $\tilde{x} = \tilde{x}_l$.[25] Consequently, except at $\tilde{x} = \tilde{x}_r$, the conservation equations of the reactants and the product in the less-viscous liquid region and in the boundary region become as follows:

$$-\rho D_l \frac{d^2 Y_j}{d\tilde{x}^2} + \rho u_0 \frac{\tilde{x}_{b-} - \tilde{x}}{\tilde{x}_{b-} - \tilde{x}_l} \frac{dY_j}{d\tilde{x}} = 0 \qquad (\tilde{x}_l < \tilde{x} < \tilde{x}_{b-}), \quad (7)$$

$$\rho D_b \frac{d^2 Y_j}{d\tilde{x}^2} = 0 \qquad (\tilde{x}_{b-} < \tilde{x} < \tilde{x}_{b+}). \quad (8)$$

Here, Y_j represents Y_l, Y_m, and Y_p, where Y_p is the mass fraction of the product. No reaction rate term is included because the reaction rate in all regions, except at $\tilde{x} = \tilde{x}_r$, is zero.

In the case of $\tilde{x}_l \le \tilde{x}_r \le \tilde{x}_{b-}$ (Figure 7a), the profiles of the mass fraction of the reactants, $Y_{l,1}$ (Y_l in Range 1: $\tilde{x}_l \le \tilde{x} \le \tilde{x}_r$), $Y_{m,2}$ (Y_m in Range 2: $\tilde{x}_r \le \tilde{x} \le \tilde{x}_{b-}$), and $Y_{m,3}$ (Y_m in Range 3: $\tilde{x}_{b-} \le \tilde{x} \le \tilde{x}_{b+}$), are obtained by solving Eqs. 7 and 8 under the boundary conditions mentioned below,

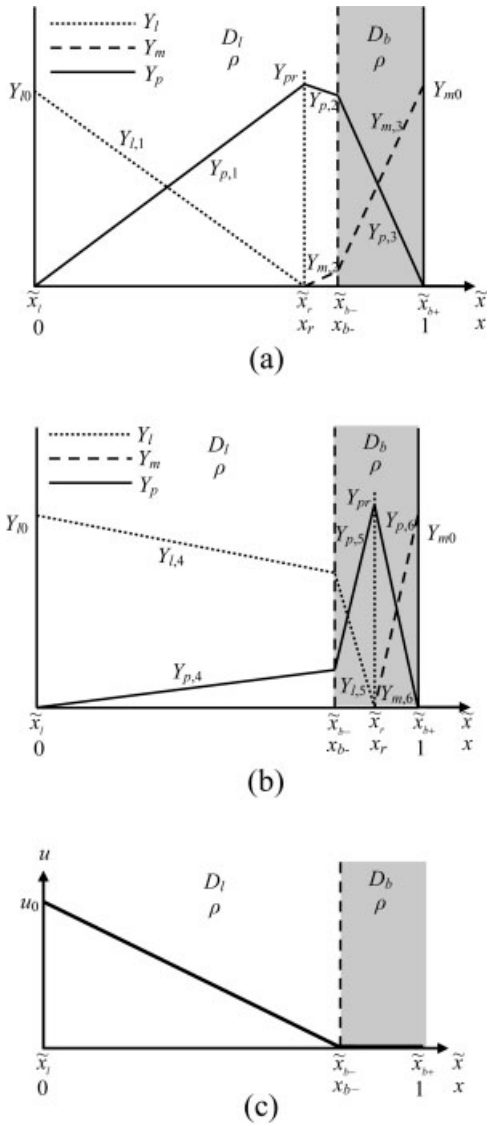

Figure 7. Schematics of the mass fraction profile of the two reactants and product for (a) $\tilde{x}_l \le \tilde{x}_r \le \tilde{x}_{b-}$ and for (b) $\tilde{x}_{b-} \le \tilde{x}_r \le \tilde{x}_{b+}$ and (c) velocity profile in the diffusive zone.

Gray region indicates the boundary region between the less- and more-viscous liquids. In (a) and (b), the mass fraction profiles are represented by straight lines, indicating the case involving no convective effect. Here, Y_{pr} is Y_p at $\tilde{x} = \tilde{x}_r$. In (c), the velocity toward the boundary, u, linearly decreases against $\tilde{x}$ under the assumption of the two-dimensional, steady, stagnated flow in the less-viscous liquid, and no velocity is assumed in the boundary region.

at $\tilde{x} = \tilde{x}_l$, $Y_{l,1} = Y_{l0}$,
at $\tilde{x} = \tilde{x}_r$, $Y_{l,1} = Y_{m,2} = 0$, and

$$-\alpha\rho D_l \frac{dY_{l,1}}{d\tilde{x}}\Big|_{\tilde{x}=\tilde{x}_r} = \rho D_l \frac{dY_{m,2}}{d\tilde{x}}\Big|_{\tilde{x}=\tilde{x}_r}, \tag{9}$$

at $\tilde{x} = \tilde{x}_{b-}$, $Y_{m,2} = Y_{m,3}$, and

$$\rho D_l \frac{dY_{m,2}}{d\tilde{x}}\Big|_{\tilde{x}=\tilde{x}_{b-}} = \rho D_b \frac{dY_{m,3}}{d\tilde{x}}\Big|_{\tilde{x}=\tilde{x}_{b-}}, \tag{10}$$

at $\tilde{x} = \tilde{x}_{b+}$, $Y_{m,3} = Y_{m0}$.
Equation 9 indicates the stoichiometric relation at $\tilde{x} = \tilde{x}_r$, which means that the ratio of the mass fluxes of reactants at $\tilde{x} = \tilde{x}_r$ is identical to the mass stoichiometric ratio of the chemical reaction, and α represents the mass stoichiometric ratio defined by $\alpha = aM_m/M_l$, where M_m is the molecular weight of the reactant initially included in the more-viscous liquid, and M_l is that initially included in the less-viscous liquid. Equation 10 indicates the mass flux continuity of the reactant at $\tilde{x} = \tilde{x}_{b-}$. In the case of $\tilde{x}_{b-} \le \tilde{x}_r \le \tilde{x}_{b+}$ (Figure 7b), the profiles of the mass fraction of reactants, $Y_{l,4}$ (Y_l in Range 4: $\tilde{x}_l \le \tilde{x} \le \tilde{x}_{b-}$), $Y_{l,5}$ (Y_l in Range 5: $\tilde{x}_{b-} \le \tilde{x} \le \tilde{x}_r$), and $Y_{m,6}$ (Y_m in Range 6: $\tilde{x}_r \le \tilde{x} \le \tilde{x}_{b+}$), are obtained by solving Eqs. 7 and 8 under the boundary conditions mentioned below,
at $\tilde{x} = \tilde{x}_l$, $Y_{l,4} = Y_{l0}$,
at $\tilde{x} = \tilde{x}_{b-}$, $Y_{l,4} = Y_{l,5}$, and

$$-\rho D_l \frac{dY_{l,4}}{d\tilde{x}}\Big|_{\tilde{x}=\tilde{x}_{b-}} = -\rho D_b \frac{dY_{l,5}}{d\tilde{x}}\Big|_{\tilde{x}=\tilde{x}_{b-}}, \tag{11}$$

at $\tilde{x} = \tilde{x}_r$, $Y_{l,5} = Y_{m,6} = 0$, and

$$-\alpha\rho D_b \frac{dY_{l,5}}{d\tilde{x}}\Big|_{\tilde{x}=\tilde{x}_r} = \rho D_b \frac{dY_{m,6}}{d\tilde{x}}\Big|_{\tilde{x}=\tilde{x}_r}, \tag{12}$$

at $\tilde{x} = \tilde{x}_{b+}$, $Y_{m,6} = Y_{m0}$.
Equations 11 and 12 are analogous to Eqs. 10 and 9, respectively.

To render Eqs. 7 and 8 and the boundary conditions mentioned above dimensionless, ρ_l, D_l, and u_0 are selected as characteristic values of density, diffusion coefficient, and velocity, respectively. As well, $\tilde{x}$ is normalized as $x = (\tilde{x} - \tilde{x}_l)/(\tilde{x}_{b+} - \tilde{x}_l)$, so that $x = 0$ and 1 correspond to $\tilde{x} = \tilde{x}_l$ and $\tilde{x} = \tilde{x}_{b+}$, respectively. In addition, $x = x_{b-}$ and $x = x_r$ correspond to $\tilde{x} = \tilde{x}_{b-}$ and $\tilde{x} = \tilde{x}_r$. The normalized coordinate x is present in Figures 7 along with $\tilde{x}$. Equations 7 and 8 for the nondimensional variables take the form, respectively,

$$\frac{d^2Y_j}{dx^2} - Pe_l \frac{1}{x_{b-}}\left(1 - \frac{x}{x_{b-}}\right)\frac{dY_j}{dx} = 0 \quad (0 \le x \le x_{b-}), \tag{13}$$

$$\frac{d^2Y_j}{dx^2} = 0 \qquad (x_{b-} \le x \le 1), \tag{14}$$

where Pe_l is the Peclet number of the chemical species transported in the less-viscous liquid region and is defined as

$$Pe_l = \frac{u_0(\tilde{x}_{b-} - \tilde{x}_l)}{D_l}. \tag{15}$$

Pe_l is proportional to u_0 because $\tilde{x}_{b-} - \tilde{x}_l$ and D_l are constant. The profiles of Y_j in the ranges of $0 \le x \le x_{b-}$ and $x_{b-} \le x \le 1$ can be analytically expressed by solving Eqs. 13 and 14, respectively, as

$$Y_j = k_1 \int_0^{1-\frac{x}{x_{b-}}} \exp\left(-\frac{Pe_l\xi^2}{2}\right)d\xi + k_2 \qquad (0 \le x \le x_{b-}), \tag{16}$$

$$Y_j = k_3 x + k_4 \qquad (x_{b-} \le x \le 1), \tag{17}$$

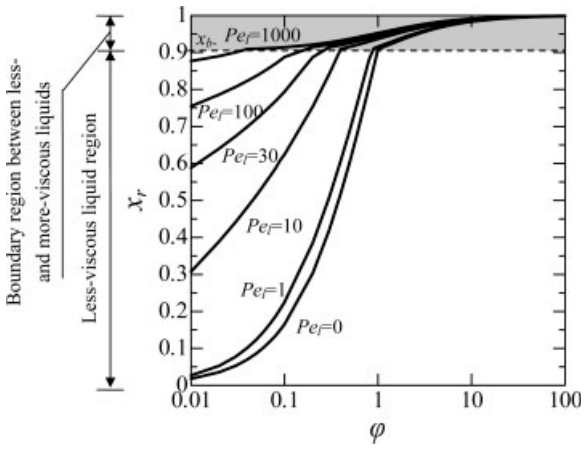

Figure 8. Variation in x_r with φ for various Pe_l.

Gray region indicates the boundary region between the less- and more-viscous liquids. Here, $x_{b-} \approx 0.909$.

where k_1–k_4 are constants of integration determined by the boundary conditions. In the present analysis, the diffusion width of the reactants and the product in the less-viscous liquid region and that of the boundary region are assumed to be proportional to the product of the values of their density and diffusivity. Thus, the following relation is satisfied:

$$\tilde{x}_{b-} - \tilde{x}_l : \tilde{x}_{b+} - \tilde{x}_{b-} = x_{b-} : 1 - x_{b-} = \rho D_l : \rho D_b, \qquad (18)$$

which leads to

$$x_{b-} = D_l/(D_l + D_b) \approx 0.909. \qquad (19)$$

The normalized location of the reaction plane, x_r, is analytically determined as functions of Pe_l and φ, for $0 \le x \le x_{b-}$ and for $x_{b-} \le x \le 1$, respectively, as follows:

$$\int_0^{1-\frac{x_r}{x_{b-}}} \exp\left(-\frac{Pe_l\xi^2}{2}\right)d\xi = \frac{\int_0^1 \exp\left(-\frac{Pe_l\xi^2}{2}\right)d\xi - \frac{\alpha Y_{l0}}{Y_{m0}}}{\frac{\alpha Y_{l0}}{Y_{m0}} + 1} = \frac{\int_0^1 \exp\left(-\frac{Pe_l\xi^2}{2}\right)d\xi - \varphi}{\varphi + 1} \quad (0 \le x \le x_{b-}), \qquad (20)$$

$$x_r = x_{b-} + \frac{(1 - x_{b-})\left\{\frac{\alpha Y_{l0}}{Y_{m0}} - \int_0^1 \exp\left(-\frac{Pe_l\xi^2}{2}\right)d\xi\right\}}{\frac{\alpha Y_{l0}}{Y_{m0}} + 1} = x_{b-} + \frac{(1 - x_{b-})\left\{\varphi - \int_0^1 \exp\left(-\frac{Pe_l\xi^2}{2}\right)d\xi\right\}}{\varphi + 1} \quad (x_{b-} \le x \le 1), \qquad (21)$$

where $\alpha Y_{l0}/Y_{m0}$ is transformed into φ by using relations such as $Y_{l0} = c_{l0}M_l/\rho$ and $Y_{m0} = c_{m0}M_m/\rho$, and Eq. 2.

Variations in x_r with φ for various Pe_l obtained by Eqs. 20 and 21 are shown in Figure 8. Here, $Pe_l = 0$ indicates no convective effect. In other words, the result at $Pe_l = 0$ is the same as that obtained by diffusion-reaction analysis. When Pe_l is small, x_r is located relatively far from x_{b-} in the less-viscous liquid region for $\varphi \ll 1$, while x_r is located in the boundary region for $\varphi \gg 1$. As Pe_l increases, x_r shifts toward x_{b-} for $\varphi \ll 1$, whereas change in x_r is scarce for $\varphi \gg 1$. These results show that even when the miscibility is taken into account, although there is a difference between the present and previous analyses[25,27] in which for $\varphi > 1$, x_r is located in the boundary region in the present analysis whereas in the more-viscous liquid region in the previous analysis, the obtained results are essentially similar to those in the previous analyses mentioned below. A significant dependence of x_r on φ takes place for small Pe_l, and as Pe_l increases, the dependence of x_r on φ decreases.

Discussion

A plausible model of the difference in the reactive flow fields depending on φ, based on the analytical results mentioned above, is shown in Figure 9. When $\varphi \ll 1$, the reaction plane, which is expected to be located relatively far from the boundary in the less-viscous liquid in the condition involving a relatively weak convective effect, cannot form along the spike because the boundary abruptly thins and the thin finger becomes quite long. This can result in the product being only negligibly distributed in the spike. In contrast, when $\varphi \gg 1$, the reaction plane can form along the spike because the reaction plane is expected to be located in the boundary, which, in turn, leads to a significant product distribution in the spike. In Figure 3, the width of the blood-red color in the spike is larger when $\varphi = 25$ than when $\varphi = 5$. This is supposed to occur because the reaction plane is located in the boundary closer to the more-viscous liquid

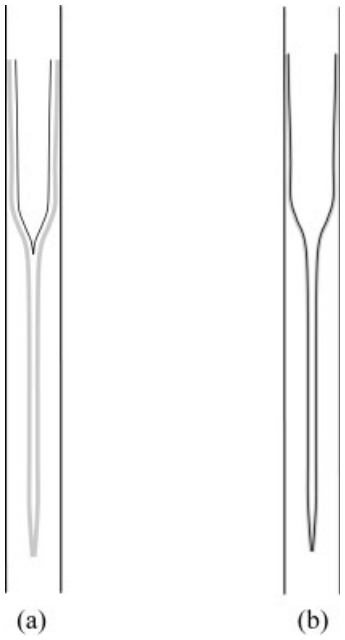

Figure 9. Proposed schematics of the reacting flow field in the presence of the spike for (a) $\varphi \ll 1$ and (b) $\varphi \gg 1$.

The wide gray lines and the thin black lines represent the boundary between the two miscible liquids and the reaction plane, respectively.

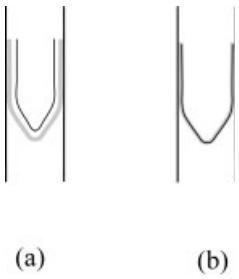

Figure 10. Proposed schematics of the reacting flow field in the absence of the spike for (a) φ << 1 and (b) φ >> 1.

The wide gray lines and the thin black lines represent the boundary between the two miscible liquids and the reaction plane, respectively.

when $\varphi = 25$ than when $\varphi = 5$, which is predicted in the analytical result shown in Figure 8.

It should be emphasized that the Péclet number used in the analysis, Pe_l, increases with that in the experiment, Pe. However, their values are not quantitatively equivalent because their definitions are different. In other words, Pe_l does not have to be 3300 in the experimental condition shown in Figures 2 and 3 where $Pe = 3300$. We recall that D and D_l in the definitions of Pe and Pe_l have values of $D \approx 1 \times 10^{-10}$ m^2/s and $D_l = 1 \times 10^{-9}$ m^2/s, respectively. With regard to the length's scale, the diameter of the tube, $d = 3$ mm, is used in the definition of Pe, while the diffusion width in the less-viscous liquid, $\tilde{x}_{b-} - \tilde{x}_l$, is used in the definition of Pe_l. We assume that the estimated diffusion width of $\sqrt{D_l t}$ is acceptable. As the value of $t = 1 \times 10^2$ s is used, the value of $\sqrt{D_l t}$ is estimated as 3×10^{-4} m. Regarding the velocity, u_0 in Pe_l is considered to be smaller than U in Pe. Therefore, it is reasonable to consider that $Pe_l \leq 0.01\ Pe$. Thus, Pe_l is considered to be smaller than 33 in the experimental condition shown in Figures 2 and 3. This indicates that the reaction plane's location is theoretically predicted to depend significantly on φ in the experimental condition of $Pe = 3300$ based on Figure 8. This result supports the model proposed in Figure 9.

Figure 10 shows schematics of the reacting flow field proposed under the condition shown in Figure 4. In this case, based on the analytical results, when $\varphi \ll 1$, the reaction plane is predicted to be located in the less-viscous liquid farther from the boundary compared to the case in Figure 3. This indicates that the difference in the locations of the reaction plane dependent on φ is expected to increase with a decrease in q or Pe in terms of the reactants' transport. In spite of this, the product distribution's dependence on φ is hardly observed in the experimental results. This is considered to be due to the negligible difference in the relationship between the locations of the boundary and the reaction plane, as shown in Figure 10. This is caused by the shape of the boundary that is almost parabolic, and thus the reaction plane is established along the boundary even when $\varphi \ll 1$. This can result in the product distribution being independent of φ. This shows that the presence of the spike is indispensable for a significant difference between the locations of the boundary and the reaction plane as induced by changes in φ, and is thus also indispensable for a significant difference in the product distribution due to φ. The experimental results shown in Figure 5 can now be understood because the difference in the locations of the boundary and the reaction plane decreases with an increase in q or Pe in terms of the reactants' transport based on the analytical results. In addition, the shape of the boundary is almost parabolic.

On the basis of the above discussion, the cause of the product distribution's significant dependence on φ can be considered as follows. Whether the reaction plane is located in either the less-viscous liquid or the boundary between the two liquids (which occurs in terms of the reactants' transport) results in the significant difference between the locations of the boundary and the reaction plane, as affected by the spike configuration of the boundary, which in turn occurs according to the principles of hydrodynamics. The location of the reaction plane's dependence on φ is caused by the diffusion coefficient between the less- and more-viscous liquids being much smaller that that of the chemical species in the less-viscous liquid. The chemical reaction induced by the two reactants initially included in glycerin and water satisfies this condition. It is considered, at the time of this writing, that a stress believed to act in a region having a steep concentration gradient between two miscible liquids, which mimics an interfacial tension acting on two immiscible fluids, plays an important role in spike formation.[6,29] The use of glycerin and water produces such a steep concentration gradient between two miscible liquids. Thus, a chemical-reacting flow involving the use of glycerin and water can be interpreted as satisfying both of the two conditions, one being that the difference is present whether the reaction plane is located in the less-viscous liquid or in the boundary due to φ in terms of transport phenomena, the other being that the boundary forms the spike according to the principles of fluid dynamics.

Comparison should be made between the experimental results of the present study using a capillary tube and the results of the previous studies[25,26] involving a Hele-Shaw cell. As mentioned in "Introduction," in the Hele-Shaw cell experiment, when finger-growth velocity is low, the product in the $R \times \theta$ plane is present in large quantities in a relatively broad area within the interior of the fingers for $\varphi_v \ll 1$, while it is concentrated around the tips of the fingers for $\varphi_v \gg 1$.[25] When finger-growth velocity is high, the product is distributed from the interior to the tip of the fingers regardless of φ_v.[26] The present results shown in Figures 3 and 5 correspond to those from the Hele-Shaw cell experiment in the cases where finger-growth velocity is low and high, respectively. It is worth noting that the experimental results corresponding to the present results (shown in Figure 4), in which the spike is not formed under the low displacement speed condition, are not observed in the previous Hele-Shaw cell experiments. We have found that the present result shown in Figure 5 is consistent with that of the previous Hele-Shaw cell experiment for the high finger-growth velocity condition. However, we have found that the present results shown in Figure 3 are not completely consistent with those of the previous Hele-Shaw cell experiment for the low finger-growth velocity condition. For small φ (or φ_v), the capillary tube's experimental results are consistent with the Hele-Shaw cell's experimental results. Actually, for small φ,

the product is scarcely observed in the spike and is clearly observed around the base of the finger in the capillary tube experiment. For large φ (or φ_v), the capillary tube's experimental results are not quite consistent with the Hele-Shaw cell's experimental results in that in the capillary tube experiment, the product is distributed significantly in the spike and around the base of the finger. In this, we see that the product distribution in the finger base for large φ (or φ_v) is the only point which differs between the Hele-Shaw cell experiment and the capillary tube experiment. Research attempting to elucidate how this difference arises is currently underway. The present study strongly suggests, however, that the formation of the sheet structure in the miscible displacement in the Hele-Shaw cell is responsible for the significant difference in the product distribution in the viscous fingering pattern in the $R \times \theta$ plane due to φ_v observed in Nagatsu and Ueda.[25]

Here, we discuss the relationship between the present reacting flow and the so-called mixing-sensitive reactions such as the four Bourne reactions,[34] in which product formation and selectivity largely depend on local reactant concentrations. In the mixing-sensitive reactions, flow condition determines the degree of mixing and thus determines the local reactant concentrations that in turn affect the product distribution. In other words, the product distribution in such cases depends not on the initial reactant concentrations (concentrations of the reactants injected to the flow field) but on flow condition. In contrast, the product distribution in the present reacting flow depends not on flow condition but on initial reactant concentrations.

In combustion, which is a typical reacting flow problem in a gas phase, the variation in the locations of the reaction plane, that is, a flame sheet in a diffusion flame due to the initial concentration of fuel, is sometimes discussed.[35] In this case, since the difference in the relationship between the location of the boundary between the fuel and oxidizer and that of the flame sheet is not significant, a remarkable difference in product distribution is not observed. Additionally, in a reacting flow in a liquid phase, especially in the case of water, the reaction plane is always located in the boundary since the diffusion coefficient between the two nonpremixed phases has the same order of magnitude (10^{-9} m^2/s) as that of the reactants in the water phase. Actually, a significant difference in the product distribution owing to initial reactant concentrations has never been discussed in such a system. To the best of our knowledge, miscible displacement with a chemical reaction involving the spike in a capillary tube, as well as that involving the sheet structure in a Hele-Shaw cell employed in the present study or in Nagatsu and Ueda,[25] is the only reacting flow in which the product distribution is significantly changed by the initial reactant concentrations.

Conclusion

Experimental and theoretical investigations have been performed regarding the miscible displacements of a more-viscous liquid by a less-viscous liquid with a chemical reaction in a capillary tube. Here, the chemical reaction is instantaneous and does not influence hydrodynamics. In the present study, we have focused on whether the formation of the spike is responsible for a significant difference in the product distribution due to the ratio between the reactant concentrations initially included in the more- and less-viscous liquids normalized by a stoichiometric ratio of the chemical reaction, φ, which is defined as $\varphi = ac_{l0}/c_{m0}$ [where c_{l0} and c_{m0} are the molar reactant concentrations initially included in the less- and more-viscous liquids, respectively, and a is the molar stoichiometric ratio of the chemical reaction ($a = 2$ in this study)]. The experimental results show that upon spike formation, the product distribution significantly depends on φ. The product is clearly observed in the spike at $\varphi \gg 1$. In contrast, it is hardly observed in the spike at $\varphi \ll 1$. In the present experimental system, we have found that the spike is not formed and the shape of the displacement tip is almost parabolic when q or Pe is decreased or increased from the condition in which the spike is formed. In both cases, the difference in product distribution due to φ is scarcely observed and the product is distributed along the boundary. We have conducted a steady convection-diffusion-reaction analysis using the system employed in the present experiments. This analysis is considered to be an improved version of the previous analyses performed by Nagatsu and Ueda[23,25] that assumes a distinct interface between two miscible fluids. In other words, the present analysis takes miscibility into account. The present analytical results show that when the convective effect is weak, the reaction plane is located relatively far from the boundary in the less-viscous liquid for $\varphi \ll 1$, while it is located in the boundary for $\varphi \gg 1$. As the convective effect increases, the location of the reaction plane is shifted toward the boundary for $\varphi \ll 1$, whereas the change in the location of the reaction plane is negligible for $\varphi \gg 1$. In other words, a significant dependence of x_r on φ takes place under a weak convective effect, and as the convective effect increases the dependence of x_r on φ decreases.

On the basis of the analytical results, a plausible model of the difference in the reactive flow fields depending of φ in cases involving a spike is proposed. In the model, when $\varphi \ll 1$, the reaction plane, which is predicted to be located relatively far from the boundary in the less-viscous liquid, cannot form along the spike because the boundary abruptly thins and the thin finger becomes quite long. In contrast, when $\varphi \gg 1$, the reaction plane can form along the spike, because the location of the reaction plane is expected to be within the boundary. The experimental results, in which the product distribution's dependence on φ is scarcely observed under the smaller q or Pe condition without the spike (although the difference in the locations of the boundary and the reaction plane due to φ is theoretically predicted to increase with a decrease in q or Pe from the viewpoint of the reactants' transport), are interpreted to be caused by the shape of the boundary that is almost parabolic, and thus the reaction plane is established along the boundary even when $\varphi \ll 1$. This shows that the spike is indispensable for the significant difference in the product distribution due to φ. The experimental results showing no difference in the product distribution due to φ under the larger q or Pe condition without the spike can be understood as follows. The difference in the locations of the boundary and the reaction plane due to φ is theoretically predicted to decrease with an increase in q or Pe in terms of the reactants' transport, while in addition the shape of the boundary is almost parabolic. To the best of our knowledge, miscible displacement with a

chemical reaction involving a spike in a capillary tube, as well as that involving the sheet structure in a Hele-Shaw cell employed in the present study or in Nagatsu and Ueda,[25] is the only reacting flow in which product distribution is significantly changed by the initial reactant concentrations.

Acknowledgment

This work is supported in part by a Sasakawa Scientific Research Grant from the Japan Science Society.

Literature Cited

1. Chouke RL, Meurs P van, Pol C van der. The instability of slow, immiscible, viscous liquid-liquid displacements in permeable media. *Trans AIME*. 1959;216:188–194.
2. Saffman PG, Taylor GI. The penetration of a fluid into a porous medium or Hele-Shaw cell containing a more viscous liquid. *Proc R Soc Lond Ser A*. 1958;245:312–329.
3. Taylor GI. Deposition of a viscous fluid on the wall of a tube. *J Fluid Mech*. 1961;10:161–165.
4. Cox BG. On driving a viscous fluid out of tube. *J Fluid Mech*. 1962;14:81–96.
5. Reinelt DA, Saffman PG. The penetration of a finger into a viscous fluid in a channel and tube. *SIAM J Sci Statis Comput*. 1985;6:542–561.
6. Petitjeans P, Maxworthy T. Miscible displacements in a capillary tube, Part 1: Experiments. *J Fluid Mech*. 1996;326:37–56.
7. Chen CY, Meiburg E. Miscible displacements in a capillary tube, Part 2: Numerical simulations. *J Fluid Mech*. 1996;326:57–90.
8. Balasubramaniam R, Rashidnia N, Maxworthy T, Kuang J. Instability of miscible interfaces in a cylindrical tube. *Phys Fluids*. 2005; 17:052103.
9. Homsy GM. Viscous fingering in porous media. *Ann Rev Fluid Mech*. 1987;19:271–311.
10. Park CW, Homsy GM. Two-phase displacement in Hele-Shaw cells: theory. *J Fluid Mech*. 1984;139:291–308.
11. Tabeling P, Zocchi G, Libchaber A. An experimental study of the Saffman-Taylor instability. *J Fluid Mech*. 1987;177:67–82.
12. Yang Z, Yortsos YC. Asymptotic solutions of miscible displacements in geometries of large aspect ratio. *Phys Fluids*. 1997;9:286–298.
13. Rakotomalala N, Salin D, Watzky P. Miscible displacement between two parallel plates: BGK lattice gas simulations. *J Fluid Mech*. 1997;388:277–297.
14. Goyal N, Meiburg E. Miscible displacements in Hele-Shaw cells: two-dimensional base states and their linear stability. *J Fluid Mech*. 2006;558:329–355.
15. Lajeunesse E, Martin J, Rakotomalala N, Salin D, Yortsos YC. Miscible displacement in a Hele-Shaw cell at high rates. *J Fluid Mech*. 1999;398:299–319.
16. Goyal N, Pichler H, Meiburg E. Variable-density miscible displacements in a vertical Hele-Shaw cell: linear stability. *J Fluid Mech*. 2007;584:357–372.
17. Hornof V, Baig FU. Influence of interfacial reaction and mobility ratio on the displacement in a Hele-Shaw cell. *Exp Fluids*. 1995;18: 448–453.
18. Broyles BS, Shalliker RA, Cherrak DE, Guiochon G. Visualization of viscous fingering in chromatographic columns. *J Chromatogr A*. 1998;822:173–187.
19. Pojman JA, Gunn G, Patterson C, Owens J, Simmons C. Frontal dispersion polymerization. *J Phys Chem B*. 1998;102:3927–3929.
20. Bhaskar KR, Garik P, Turner BS, Bradley JD, Bansil R, Stanley HE, LaMont JT. Viscous fingering of HCl through gastric mucin. *Nature*. 1992;360:458–461.
21. Fernandez J, Homsy GM. Viscous fingering with chemical reaction: effect of in-situ production of surfactants. *J Fluid Mech*. 2003;480: 267–281.
22. DeWit A, Homsy GM. Viscous fingering in reaction-diffusion systems. *J Chem Phys*. 1999;110:8663–8675.
23. DeWit A, Homsy GM. Nonlinear interaction of chemical reactions and viscous fingering in porous media. *Phys Fluids*. 1999;11:949–951.
24. Nagatsu Y, Matsuda K, Kato Y, Tada Y. Experimental study on miscible viscous fingering involving viscosity changes induced by variations in chemical species concentrations due to chemical reactions. *J Fluid Mech*. 2007;571:475–493.
25. Nagatsu Y, Ueda T. Effects of reactant concentrations on reactive miscible viscous fingering. *AIChE J*. 2001;47:1711–1720.
26. Nagatsu Y, Ueda T. Effects of finger-growth velocity on reactive miscible viscous fingering. *AIChE J*. 2003;49:789–792.
27. Nagatsu Y, Ueda T. Analytical study of effects of finger-growth velocity on reaction characteristics of reactive miscible viscous fingering by using a convection-diffusion-reaction model. *Chem Eng Sci*. 2004;59:3817–3826.
28. Tan CT, Homsy GM. Simulation of nonlinear viscous fingering in miscible displacement. *Phys Fluids*. 1988;31:1330–1338.
29. Kuang J, Petitjeans P, Maxworthy T. Velocity fields and streamline patterns of miscible displacements in cylindrical tubes. *Exp Fluids*. 2004;37:301–308.
30. Bird RB, Stewart WE, Lightfoot EN. Transport Phenomena, 2nd ed. New York: John Wiley and Sons, 2002.
31. Wilke CR, Chang P. Correlation of diffusion coefficients in dilute solutions. *AIChE J*. 1955;1:264–270.
32. Schlichting H. Boundary-Layer Theory, 7th ed. New York: McGraw-Hill, 1979.
33. Fendell FE. Ignition and extinction in combustion of initially unmixed reactants. *J Fluid Mech*. 1965;21:281–303.
34. Baldyga J, Bourne JR. *Turbulent Mixing and Chemical Reaction*. Chichester: John Wiley & Sons, 1999.
35. Tsuji H, Yamaoka I. The counterflow diffusion flame in the forward stagnation region of a porous cylinder. *Eleventh Symp (Int) on Combustion*. 1967:979–984.

Appendix: On Calculation of c_{l0} and c_{m0} in Table 1

In Figure 7, in the case of $\tilde{x}_l \le \tilde{x}_r \le \tilde{x}_{b-}$ (Figure 7a), the profiles of the mass fraction of the product, $Y_{p,1}$ (Y_p in Range 1), $Y_{p,2}$ (Y_p in Range 2), and $Y_{p,3}$ (Y_p in Range 3), are obtained by solving Eqs. 7 and 8 under the boundary conditions mentioned below;

at $\tilde{x} = \tilde{x}_l$, $Y_{p,1} = 0$.

at $\tilde{x} = \tilde{x}_r$, $Y_{p,1} = Y_{p,2} = Y_{pr}$, and

$$-\rho D_l \frac{dY_{l,1}}{d\tilde{x}}\Big|_{\tilde{x}=\tilde{x}_r} + \rho D_l \frac{dY_{m,2}}{d\tilde{x}}\Big|_{\tilde{x}=\tilde{x}_r} = \left(\rho D_l \frac{dY_{p,1}}{d\tilde{x}}\Big|_{\tilde{x}=\tilde{x}_r} - \rho u_r Y_{pr}\right) - \left(\rho D_l \frac{dY_{p,2}}{d\tilde{x}}\Big|_{\tilde{x}=\tilde{x}_r} + \rho u_r Y_{pr}\right). \tag{A1}$$

at $\tilde{x} = \tilde{x}_{b-}$, $Y_{p,2} = Y_{p,3}$, and

$$-\rho D_l \frac{dY_{p,2}}{d\tilde{x}}\Big|_{\tilde{x}=\tilde{x}_{b-}} = -\rho D_b \frac{dY_{p,3}}{d\tilde{x}}\Big|_{\tilde{x}=\tilde{x}_{b-}}. \tag{A2}$$

at $\tilde{x} = \tilde{x}_{b+}$, $Y_{p,3} = 0$.

Here, Y_{pr} is Y_p at $\tilde{x} = \tilde{x}_r$. Equation A1 indicates the mass conservation of the reactants and the product at $\tilde{x} = \tilde{x}_r$, which means that the sum of the mass fluxes of the reactants into the reaction plane is equal to that of the product from the reaction plane. Here, u_r is u at $\tilde{x} = \tilde{x}_r$. Equation A2 indicates the mass flux continuity of the product at $\tilde{x} = \tilde{x}_{b-}$. In the case of $\tilde{x}_{b-} \le \tilde{x}_r \le \tilde{x}_{b+}$ (Figure 7b), the profiles of the mass fraction of the product, $Y_{p,4}$ (Y_p in Range 4), $Y_{p,5}$ (Y_p in Range 5), and $Y_{p,6}$ (Y_p in Range 6), are obtained by solving Eqs. 7 and 8 under the boundary conditions mentioned below,

at $\tilde{x} = \tilde{x}_{\mathrm{l}}$, $Y_{\mathrm{p},4} = 0$.
at $\tilde{x} = \tilde{x}_{\mathrm{b}-}$, $Y_{\mathrm{p},4} = Y_{\mathrm{p},5}$, and

$$\rho D_{\mathrm{l}} \frac{dY_{\mathrm{p},4}}{d\tilde{x}}|_{\tilde{x}=\tilde{x}_{\mathrm{b}-}} = \rho D_{\mathrm{b}} \frac{dY_{\mathrm{p},5}}{d\tilde{x}}|_{\tilde{x}=\tilde{x}_{\mathrm{b}-}}. \tag{A3}$$

at $\tilde{x} = \tilde{x}_{\mathrm{r}}$, $Y_{\mathrm{p},5} = Y_{\mathrm{p},6} = Y_{\mathrm{pr}}$, and

$$-\rho D_{\mathrm{m}} \frac{dY_{\mathrm{l},5}}{d\tilde{x}}|_{\tilde{x}=\tilde{x}_{\mathrm{r}}} + \rho D_{\mathrm{m}} \frac{dY_{\mathrm{m},6}}{d\tilde{x}}|_{\tilde{x}=\tilde{x}_{\mathrm{r}}} = \rho D_{\mathrm{m}} \frac{dY_{\mathrm{p},5}}{d\tilde{x}}|_{\tilde{x}=\tilde{x}_{\mathrm{r}}} - \rho D_{\mathrm{m}} \frac{dY_{\mathrm{p},6}}{d\tilde{x}}|_{\tilde{x}=\tilde{x}_{\mathrm{r}}}. \tag{A4}$$

at $\tilde{x} = \tilde{x}_{\mathrm{b}+}$, $Y_{\mathrm{p},6} = 0$.
Equations A3 and A4 are analogous to Eqs. A2 and A1, respectively. Y_{pr} is determined by Eq. A5 employing Eqs. A1, A2, 19, and 20 in the case of $\tilde{x}_{\mathrm{l}} \leq \tilde{x}_{\mathrm{r}} \leq \tilde{x}_{\mathrm{b}-}$, or by using Eqs. A3, A4, 19, and 21 in the case of $\tilde{x}_{\mathrm{b}-} \leq \tilde{x}_{\mathrm{r}} \leq \tilde{x}_{\mathrm{b}+}$,

$$Y_{\mathrm{pr}} = \frac{(\alpha+1) Y_{\mathrm{l}0} Y_{\mathrm{m}0}}{\alpha Y_{\mathrm{l}0} + Y_{\mathrm{m}0}}. \tag{A5}$$

The molar concentration of the product, c_{pr}, is determined by Eq. A6,

$$c_{\mathrm{pr}} = \frac{\rho Y_{\mathrm{pr}}}{M_{\mathrm{p}}} = \frac{c_{\mathrm{l}0} c_{\mathrm{m}0}}{a c_{\mathrm{l}0} + c_{\mathrm{m}0}}, \tag{A6}$$

where M_{p} is the molecular weight of the product. In the present experimental conditions shown in Table 1, $c_{\mathrm{l}0}$ and $c_{\mathrm{m}0}$ are determined such that c_{pr} in Eq. A6 is identical for each φ condition.

Manuscript received July 27, 2007, and revision received Nov. 8, 2007.